Design and Electronic Structure of New Styryl Dye Bases: Steady-State and Time-Resolved Spectroscopic Studies

ARTICLE *in* THE JOURNAL OF PHYSICAL CHEMISTRY A · JUNE 2014

Impact Factor: 2.69 · DOI: 10.1021/jp503263f · Source: PubMed

11 AUTHORS, INCLUDING:

Artem E. Masunov

University of Central Florida

147 PUBLICATIONS **2,538** CITATIONS

SEE PROFILE

Julia Bricks

National Academy of Sciences of Ukraine

69 PUBLICATIONS **1,026** CITATIONS

SEE PROFILE

Yu. P. Piryatinski

National Academy of Sciences of Ukraine

51 PUBLICATIONS **203** CITATIONS

SEE PROFILE

Kevin D Belfield

University of Central Florida

225 PUBLICATIONS **4,279** CITATIONS

SEE PROFILE

THE JOURNAL OF PHYSICAL CHEMISTRY A

Article

pubs.acs.org/JPCA

Design and Electronic Structure of New Styryl Dye Bases: Steady-State and Time-Resolved Spectroscopic Studies

N. V. Bashmakova,[†,‡] Ye. O. Shaydyuk,[†] S. M. Levchenko,[†,§] A. E. Masunov,*[,∥,⊥,#] O. V. Przhonska,[†] J. L. Bricks,[▼] O. D. Kachkovsky,[▼] Yu. L. Slominsky,[▼] Yu. P. Piryatinski,[†] K. D. Belfield,[⊥,¶] and M. V. Bondar*[,†]

[†]Institute of Physics, Prospect Nauki, 46, Kyiv-28 03028, Ukraine

[‡]Taras Shevchenko National University of Kyiv, Volodymyrska Street, 60, Kyiv 01601, Ukraine

[§]Institute of Molecular Biology and Genetics, 150, Akademika Zabolotnoho Strasse, Kyiv 036803, Ukraine

[∥]NanoScienece Technology Center, [⊥]Department of Chemistry, [#]Department of Physics, and [¶]CREOL, The College of Optics and Photonics, University of Central Florida, P.O. Box 162366, Orlando, Florida 32816, United States

[▼]Insitute of Organic Chemistry, Murmanskaya Street, 5, Kyiv 03094, Ukraine

ABSTRACT: A comprehensive investigation of the electronic structure and fast relaxation processes in the excited states of new styryl base-type derivatives was performed using steady-state, pico-, and femtosecond time-resolved spectroscopic techniques. Linear photophysical parameters of new compounds, including steady-state absorption, fluorescence, and excitation anisotropy spectra, were obtained in a number of organic solvents at room temperature. A detailed analysis of the fluorescence lifetimes and ultrafast relaxation processes in the electronically excited state of the styryl bases revealed an important role of solvate dynamics and donor−acceptor strength of the molecular structures in the formation of their excited state absorption spectra. Experimental data were in good agreement with quantum chemical calculations at the time dependent density functional theory level, combined with a polarizable continuum model.

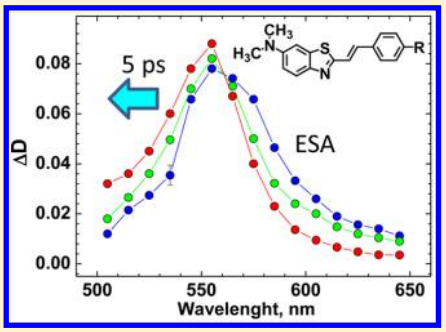

1. INTRODUCTION

Styryl-based neutral compounds with the general molecular structure D-π-D and D-π−A (D, A, and π are the electron-donating, electron-accepting, and π-conjugated systems, respectively) are one of the most frequently used types of organic dyes[1−3] with high potential for manifold practical applications, including biosensing and bioimaging,[4] organic photovoltaics,[5] ion detection,[6] lasing,[7] etc. Linear photophysical, time-resolved spectroscopic, and nonlinear optical properties of this type of organic compounds are scarcely addressed in the scientific literature and, therefore, are a subject of great interest. A comprehensive photophysical study of 15-crown-5-substituted styryl bases was performed in liquid organic medium at room temperature,[6] and specific cation-sensitive changes in the observed fluorescence emission were shown under the complexation processes. The effects of solvent parameters on the fluorescence and isomerization quantum yields of styrylbenzoxazole derivatives were revealed along with the important role of the intramolecular charge transfer in controlling the electronic properties of the ground and excited states.[8] The hole mobility and general photophysical properties were determined for styryl-substituted poly(*p*-phenyleneethynylene)-*alt*-poly(*p*-phenylene-vinylene)s,[5] where bis(styryl) side groups play a dominant role in the formation of charge carriers flux. The synthesis and in vitro and in vivo evaluations of two styryl-based derivatives were performed by Chang et al.,[3] and the potential of the in vivo bioimaging agents was shown for Alzheimer's disease diagnostics.

In this paper new styryl bases *N,N*-dimethyl-2-(2-phenylvinyl)-1,3-benzothiazol-6-amine (**1**), 2-[2-(4-methoxyphenyl)-vinyl]-*N,N*-dimethyl-1,3-benzothiazol-6-amine (**2**), and *N,N*-dimethyl-2-{2-[4-(trifluoromethyl)phenyl]vinyl}-1,3-benzothiazol-6-amine (**3**) were synthesized and comprehensively investigated with the steady-state and time-resolved pico- and femtosecond techniques. The peculiarities of the electronic structures of **1**−**3** responsible for the large Stokes shifts, specific solvatochromic behavior, and fast relaxations in the excited states were revealed. Linear spectral data were in good agreement with quantum chemical calculations based on density functional theory performed with the use of the Gaussian 2009 suite of programs.[9]

2. EXPERIMENTAL SECTION

2.1. Materials and Methods. The series of styryl bases reported here were prepared by traditional method comprehensively described previously.[6,10] This method involves heating of a mixture of 6-dimethylamino-2-methylbenzothiazole and the corresponding 4(*R*)-substituted benzaldehyde in

Received: April 2, 2014
Revised: May 28, 2014

dx.doi.org/10.1021/jp503263f | *J. Phys. Chem. A* XXXX, XXX, XXX−XXX

dimethyl sulfoxide solution. Structures of all synthesized dyes are presented in Figure 1. The structure and purity of the dyes

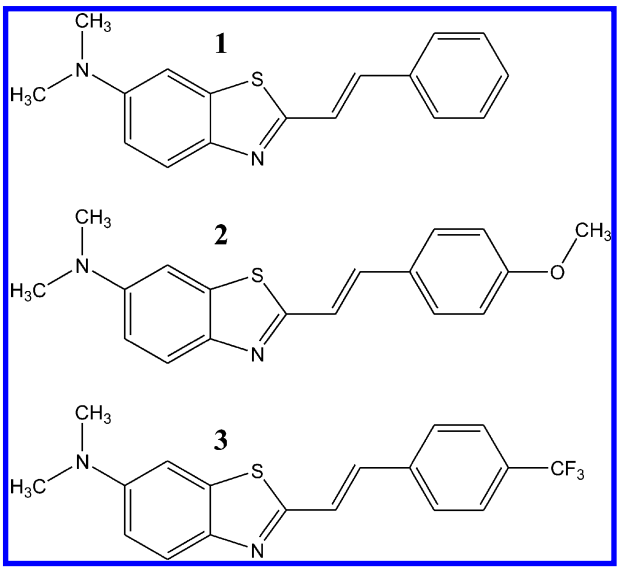

Figure 1. Molecular structures of the investigated styryl bases **1**−**3**.

were confirmed by NMR spectroscopy and elemental analysis. Starting materials and solvents for the synthesis and spectroscopic measurements were purchased from Sigma-Aldrich.

General Synthetic Procedure for Styryl Bases. A mixture of 3 mmol of 6-dimethylamino-2-methylbenzothiazole, 3.3 mmol of 4-substituted benzaldehyde, and 0.2 g of powdered potassium hydroxide was heated in 3 mL of DMSO at 50 °C producing a solution, then at 70 °C for 3 h. After cooling to room temperature, 40 mL of water was added. A solid precipitated was filtered off, washed with water, dried, and recrystallized from an appropriate solvent.

*N,N-Dimethyl-2-(2-phenylvinyl)-1,3-benzothiazol-6-amine (**1**).* Yield 36%, mp 146−148 °C (recrystallized from acetonitrile). ^{1}H NMR ($CDCl_3$) δ (ppm): 3.032 (s, 6H), 6.93 (dd, J = 9.5, 2.5 Hz, 1H), 7.08 (s bright, 1H), 7.33 (m, 1H), 7.38 (m, 4H), 7.55 (d, J = 8.5 Hz, 2H), 7.82 (d, J = 9 Hz, 1H). Elemental analysis calcd. (%) for $C_{17}H_{16}N_2S$ (280.39): C 72.82, H 5.75, N 9.99; found: C 72.58, H 5.62, N 10.08.

*2-[2-(4-Methoxyphenyl)vinyl]-N,N-dimethyl-1,3-benzothiazol-6-amine (**2**).* Yield 63%, mp 147−151 °C (recrystallized from ethanol). ^{1}H NMR (CD_3CN) δ (ppm): 2.99 (s, 6H), 3.82 (s, 3H), 6.96 (m, 3H), 7.19 (d, J = 2.4 Hz, 1H), 7.26 (d, J = 16.2 Hz, 1H), 7.37 (d, J = 16.2 Hz, 1H), 7.58 (m, 2H), 7.72 (d, J = 9.0 Hz, 1H). Elemental analysis calcd. (%) for $C_{18}H_{18}N_2OS$ (310.40): C 69.65, H 5.84; found: C 69.22, H 5.87.

*N,N-Dimethyl-2-{2-[4-(trifluoromethyl)phenyl]vinyl}-1,3-benzothiazol-6-amine (**3**).* Yield 44%, mp 156−157 °C (recrystallized from ethanol). ^{1}H NMR (CD_3CN) δ (ppm): 3.02 (s, 6H), 7.00 (dd, J = 9.0, 2.1 Hz, 1H), 7.21 (d, J = 2.1 Hz, 1H), 7.45 (d, J = 16.2 Hz, 1H), 7.54 (d, J = 16.2 Hz, 1H), 7.71 (d, J = 8.7 Hz, 2H), 7.76 (s, 1H), 7.81 (d, J = 8.7 Hz, 2H). ^{19}F NMR ($CDCl_3$) δ (ppm): −63.36. Elemental analysis calcd. (%) for $C_{18}H_{15}F_3N_2S$ (348.38): C 62.05, H 4.34; found: C 61.92, H 4.42.

2.2. Steady-State Photophysical Measurements. Steady-state linear absorption, fluorescence, and excitation anisotropy spectra of **1**−**3** were measured in spectroscopic grade toluene (TOL), dichloromethane (DCM), and acetonitrile (ACN) at room temperature. Linear absorption spectra were obtained with a Shimadzu 2450 UV−visible spectrophotometer in 10 mm path length quartz cuvettes with dye concentrations $C \sim (3-5)\cdot10^{-5}$ M. The steady-state fluorescence and excitation anisotropy spectra were measured with a CM 2203 spectrofluorimeter (Solar, Belarus) in 10 mm path length spectrofluorometric quartz cuvettes with $C \sim 10^{-6}$ M. All fluorescence spectra were corrected for the spectral responsivity of the emission monochromator and PMT detection system of the spectrofluorimeter. The excitation anisotropy spectra, $r(\lambda)$, were obtained in viscous polyTHF (pTHF) using an "L-format" experimental configuration.[11] It should be mentioned that in viscous pTHF the value of molecular rotational correlation time, $\theta \gg \tau_{fl}$ (τ_{fl} is the fluorescence lifetime of the dye), and the experimentally observed anisotropy, r, was close to the fundamental value, r_0; i.e., $r = r_0/(1+\tau_{fl}/\theta) \approx r_0$. The fundamental anisotropy, r_0, was determined by the angle θ between absorption $S_0 \rightarrow S_1$ and emission $S_1 \rightarrow S_0$ transition dipoles:[11]

$$r_0 = (3\cos^2 \alpha - 1)/5 \quad (1)$$

(S_0 and S_1 are the ground and first excited electronic state, correspondingly.) In the case of small values of α, fundamental anisotropy can be used for the analysis of mutual space orientation of the transition dipoles $S_0 \rightarrow S_n$ (n = 1, 2, 3...).[12,13] Fluorescence quantum yields of **1**−**3** were determined by standard relative methodology with 9,10-diphenylanthracene in cyclohexane as a reference.[11]

2.3. Time-Resolved Spectral Measurements. Fluorescence decay curves and corresponding lifetimes, τ_{fl}, of **1**−**3**

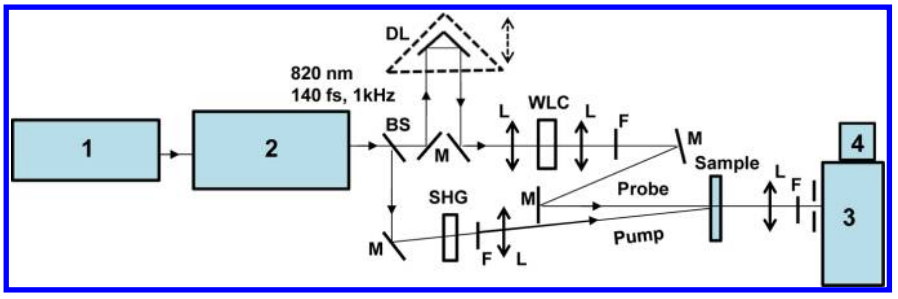

Figure 2. Simplified scheme of the experimental setup: 1, femtosecond laser Mira Optima 900-F; 2, regenerative amplifier Legent F-1K-HE; BS, beam splitter; M, 100% reflection mirrors; DL, optical delay line M-531.DD with retroreflector; SHG, second harmonic generator (1 mm BBO crystal); L, focusing lenses; F, set of neutral and/or interferometric filters; WLC, white-light continuum generator (4 mm sapphire plate); sample, 1 mm flow cell with sample solution; 3, monochromator; 4, CCD detector.

dx.doi.org/10.1021/jp503263f | J. Phys. Chem. A XXXX, XXX, XXX−XXX

were measured in a single photon counting regime using Life Spec-II spectrometer (Edinburgh Instruments Ltd.) with ≈100 ps time resolution. Fast relaxation processes in the ground and excited states were investigated by a femtosecond transient absorption pump−probe technique described in detail previously.[14,15] A representation of the simplified experimental setup is shown in Figure 2. The output of a mode-locked femtosecond Ti:sapphire laser (Mira Optima 900-F) was tuned to 820 nm and regeneratively amplified by a Legend F-1K-HE (all lasers from Coherent, Inc.), delivering a pulse train with 1 kHz repetition rate, pulse energy, $E_p \approx 1.5$ mJ, and pulse duration, $\tau_p \approx 140$ fs (fwhm). This laser beam was divided in two parts: the first one was converted into the second harmonic (410 nm, 1 mm BBO crystal) and used as a pump source with $E_p \leq 10$ μJ. The second part was focused into a 4 mm sapphire plate to produce white-light continuum (WLC) pulses, which were employed as a broadband probe source with $E_p \leq 10$ nJ. The probe pulse was delayed relative to the pump using an optical delay line (M-531.DD, PI, Inc.) with a retroreflector. The pump and probe laser beams were focused to the waists of radii ≈0.5 and ≈0.2 mm, respectively, and recombined at a small angle (<5°) in a 1 mm path length flow cell with the sample solution. The transmittance of the probe beam passing through the sample cell and corresponding transient absorption spectra of **1**−**3** were determined with an Acton SP500i spectrometer coupled with a Spec 10 CCD detector. The temporal resolution of the employed pump−probe setup was estimated as ≤500 fs.

2.3. Computational Details. All calculations were performed using the Gaussian 2009 suite of programs.[9] Density functional theory (DFT) with M05-QX exchange-correlation functional and D95 basis set[16] were used for geometry optimization. The M05-QX functional (formerly known as M05−11/4X) was derived[17] by interpolation between M05 and M05-2X functionals[18] to include 35% of the exact exchange. We had chosen to use this functional as it more accurately predicts the energies of the electronic states with higher charge transfer character, when compared to the more commonly used functionals (such as B3LYP). It was repeatedly shown to improve description of both lowest and higher excited states in polar chromophores.[19−22] The basis set with no diffusion functions was chosen in order to prevent the artifactual Rydberg contributions into the valent excited states, as described in refs 23 and 24. Time dependent density functional theory (TD-DFT)[25] was used to describe excited states. Absorption and emission spectra were predicted using optimized ground and first singlet excited state geometry, respectively. Polarizable continuum model (PCM) in solvent model density (SMD) parametrization[26] was employed to implicitly account for solvent effects (nonequilibrium for absorption and equilibrium for emission spectra). The absorption was predicted using the nonequilibrium solvation model, where charge distribution of the solute in the ground state generates orientational self-consistent reaction field in polarizable continuum. The emission was predicted using equilibrium solvation model, where the excited state of the solute generates the solvent orientational response. This reaction field, however, stabilizes both ground and excited states, and the difference in ground and excited state stabilization is responsible for predicted solvatochromic shift.

3. RESULTS AND DISCUSSION

3.1. Linear Photophysical Properties of 1−3. Linear absorption, fluorescence, and excitation anisotropy spectra, along with the main photophysical parameters of **1**−**3**, are presented in Figure 3 and Table 1, respectively. According to

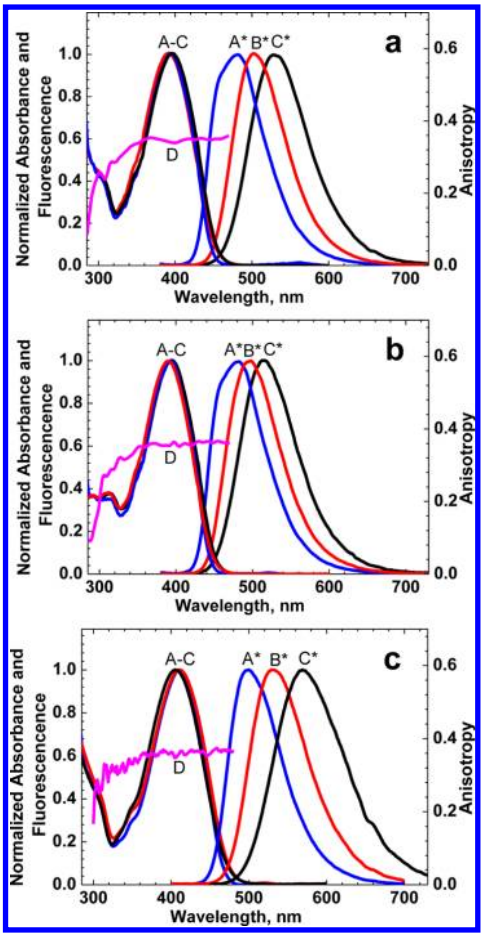

Figure 3. Linear absorption (A−C), steady-state fluorescence (A*−C*), and excitation anisotropy (D) spectra of **1** (a), **2** (b), and **3** (c) in TOL (A, A*), DCM (B, B*), and ACN (C, C*).

Figure 3 (curves A−C), the steady-state absorption spectra were practically independent of solvent polarity and revealed structureless and relatively weak long wavelength absorption bands (maximum extinction coefficient, $\varepsilon^{max} \sim (24-33)\cdot 10^3$ M^{-1} cm^{-1}). Weak solvent dependence of **1**−**3** can be explained by similar energy stabilization of the ground S_0 and Franck−Condon state of S_1, which is corresponded to the ground state optimized geometry. The steady-state fluorescence spectra (curves A*−C*) were independent of excitation wavelength and exhibited a moderate solvatochromic effect with Stokes shifts of ∼4000−7000 cm^{-1}. Large value Stokes shifts, even in a nonpolar solvent (TOL), is indicative of a strong rearrangement of the optimal molecular geometry in the excited state of **1**−**3**. It should be mentioned that direct correlation between the value of solvatochromic shift and acceptor strength of the phenyl substituents in **1**−**3** was observed, which is the distinguishing feature of the investigated styryl dye bases. A constant value of the excitation anisotropy $r(\lambda)$ in the spectral range $\lambda > 360$ nm (Figure 3, curves D) revealed a simple electronic structure of the main long wavelength absorption band of **1**−**3**, which can be attributed to a single $S_0 \rightarrow S_1$

dx.doi.org/10.1021/jp503263f | J. Phys. Chem. A XXXX, XXX, XXX−XXX

Table 1. Main Photophysical Parameters of 1−3 in Solvents of Different Polarity Δf: Absorption λ_{ab}^{max} and Fluorescence λ_{fl}^{max} Maxima, Stokes Shifts, Maximum Extinction Coefficients ε^{max}, Fluorescence Quantum Yields Φ_{fl}, and Experimental τ_{fl} and Calculated τ_{fl}^{cal} Lifetimes

solvent	TOL			DCM			ACN		
compd	1	2	3	1	2	3	1	2	3
λ_{ab}^{max}, nm	394 ± 1	393 ± 1	410 ± 1	397 ± 1	394 ± 1	410 ± 1	390 ± 1	389 ± 1	405 ± 1
λ_{fl}^{max}, nm	480 ± 1	480 ± 1	499 ± 1	502 ± 1	496 ± 1	531 ± 1	530 ± 1	515 ± 1	569 ± 1
Stokes shift, nm (cm^{-1})	86 ± 2 (4550)	87 ± 2 (4610)	89 ± 2 (4350)	105 ± 2 (5270)	102 ± 2 (5220)	121 ± 2 (5560)	140 ± 2 (6770)	126 ± 2 (6290)	164 ± 2 (7120)
$\varepsilon^{max}\cdot10^{-3}$, $M^{-1}\cdot cm^{-1}$	–	–	–	24.3 ± 2	29.5 ± 2	26.0 ± 2	27.4 ± 2	33.0 ± 2	27.0 ± 2
Φ_{fl}, %	48 ± 3	50 ± 3	47 ± 3	54 ± 3	51 ± 3	53 ± 3	45 ± 3	48 ± 3	40 ± 3
τ_{fl}, ns	2.4 ± 0.1	2.2 ± 0.1	2.8 ± 0.1	3.3 ± 0.1	2.9 ± 0.1	3.5 ± 0.1	3.6 ± 0.1	3.2 ± 0.1	3.9 ± 0.1
τ_{fl}^{cal}, ns	–	–	–	2.3 ± 0.2	1.8 ± 0.2	2.0 ± 0.2	2.0 ± 0.2	1.7 ± 0.2	2.1 ± 0.2
Δf^{a}		0.0135			0.217			0.305	

[a]Polarity (orientation polarizability) $\Delta f = (\varepsilon - 1)/(2\varepsilon + 1) - (n^2 - 1)/(2n^2 + 1)$ (ε and n are the dielectric constant and refraction index of the solvent, respectively).[11]

electronic transition. A high absolute value $r(\lambda) \geq 0.35$ is close to the theoretical limit for an isotropic molecular ensemble (r = 0.4)[11] and indicates nearly parallel orientation of the absorption $\boldsymbol{\mu}_{01}$ ($S_0 \rightarrow S_1$) and emission $\boldsymbol{\mu}_{10}$ ($S_1 \rightarrow S_0$) transition dipole moments. Fluorescence decay processes in **1**−**3** exhibited a single exponential profile (Figure 4) with corresponding

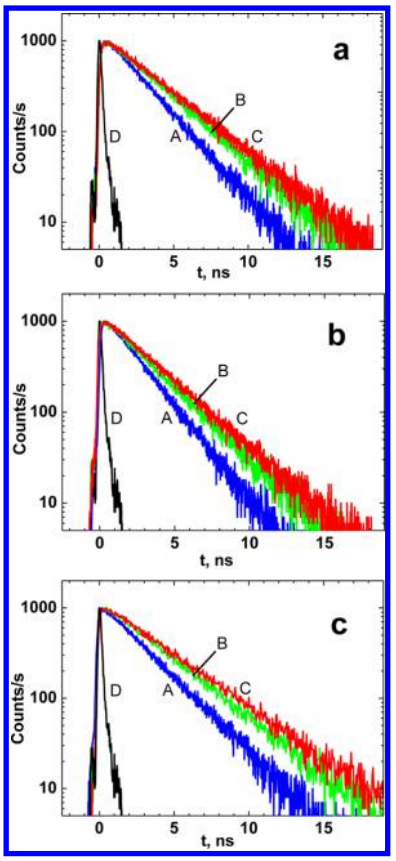

Figure 4. Fluorescence decay curves of **1** (a), **2** (b), and **3** (c) in TOL (A), DCM (B), ACN (C), and instrument response function (D).

lifetimes, τ_{fl}, in the range of 2.2−3.9 ns (Table 1). The largest value of τ_{fl} was observed for the D-π-A structure of **3** in polar ACN. A monotonic increase in τ_{fl} with solvent polarity, Δf, was shown for all these compounds (Table 1). Fluorescence lifetimes of **1**−**3** were also determined numerically from the equation $\tau_{fl}^{cal} = \tau_N \cdot \Phi_{fl}$, where the natural lifetime, τ_N, can be calculated from the Strickler−Berg approach as[27]

$$\tau_N^{-1} = 2.88\cdot10^{-9} n^2 \varepsilon^{max} \frac{\int F(\nu)d\nu \cdot \int \frac{\varepsilon(\nu)}{\nu} d\nu}{\int \frac{F(\nu)}{\nu^3} d\nu}$$

where ε^{max} is the maximum extinction coefficient of the main long wavelength absorption band (in $M^{-1}\cdot cm^{-1}$), $F(\nu)$ and $\varepsilon(\nu)$ are the normalized fluorescence and absorption spectra (plotted in wavenumbers, ν, in cm^{-1}), and n is the refractive index of the solvent. Calculated values of τ_{fl}^{cal} are presented in Table 1 and revealed a noticeable deviation from the corresponding experimental ones τ_{fl}, which indicates a relatively low intensity of $S_0 \rightarrow S_1$ singlet−singlet transitions and sufficiently large changes in the optimized geometry of the excited states.[27] Fluorescence quantum yields, Φ_{fl}, of **1**−**3** were in the range ~40−55% and exhibited a weak dependence on solvent polarity. Different donor−acceptor strength of the end

dx.doi.org/10.1021/jp503263f | J. Phys. Chem. A XXXX, XXX, XXX−XXX

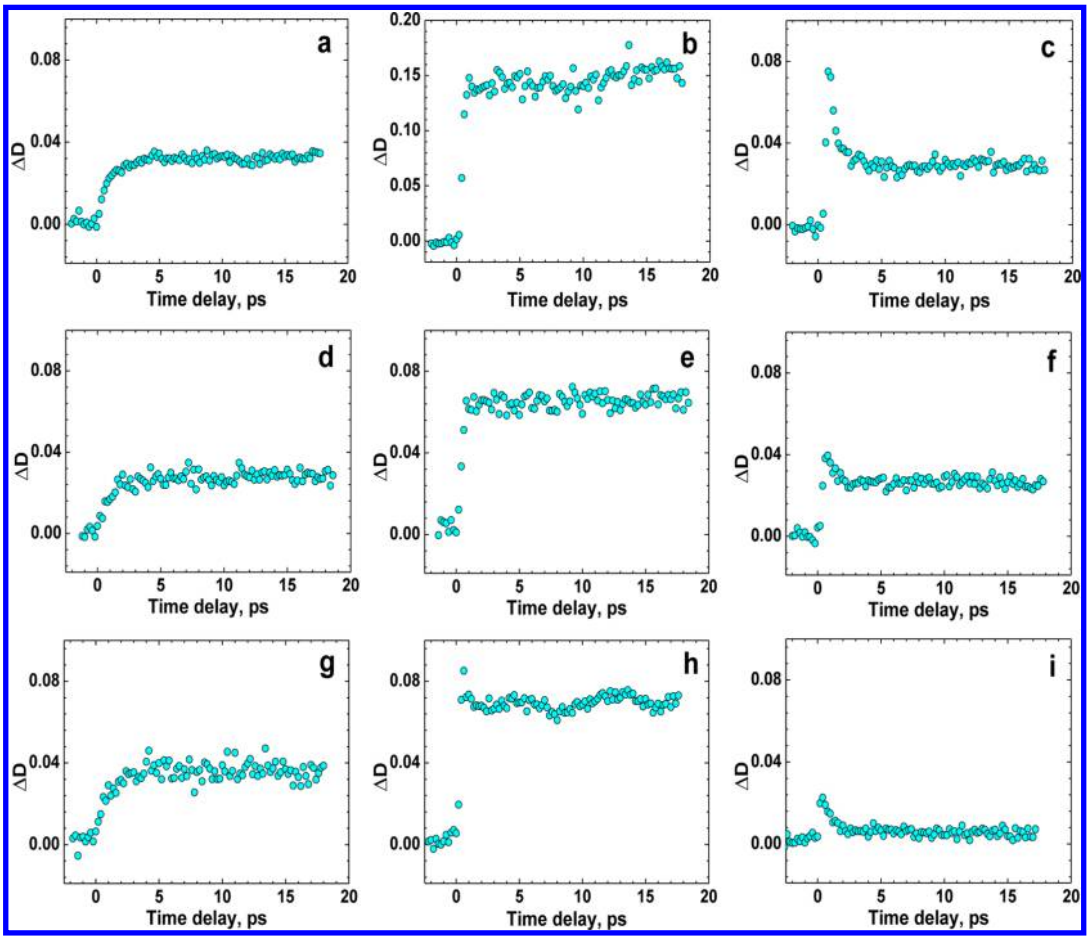

Figure 5. Transient absorption dependences $\Delta D = f(\tau_D)$ for **1** (a, b, c), **2** (d, e, f), and **3** (g, h, i) in ACN: λ_{pr} = 495 nm (a), 545 nm (b), 575 nm (c), 505 nm (d), 525 nm (e), 625 nm (f), 515 nm (g), 565 nm (h), and 615 nm (i).

substituents in the para position on benzene ring for **1**−**3** did not essentially change the corresponding values of Φ_{fl}. It should be mentioned that the three styryl bases studied here are sufficiently rigid planar structures with only one trans configuration, consistent with the observed fluorescence decay, quantum yields, and quantum chemical calculations (see section 3.3).

3.2. Femtosecond Pump−Probe Spectroscopy of Styryl Dye Bases 1−3. The nature of fast relaxation processes in the excited state of **1**−**3** was investigated in polar ACN under $S_0 \rightarrow S_1$ femtosecond excitation. Transient absorption dependences $\Delta D = f(\tau_D)$ (ΔD and τ_D are the induced optical density and time delay between pump and probe pulses, respectively) are presented in Figure 5 for various probing wavelengths, λ_{pr}, from a spectrally broad WLC probe. In general, values of ΔD are determined by saturable absorption (SA), excited state absorption (ESA), and stimulated emission (gain) processes commonly observed in organic molecules.[28−30] In the spectral range of the main absorption band (360 nm $\leq \lambda_{pr} \leq$ 440 nm, not shown in Figure 5), only negative values of ΔD were observed and all fast relaxation processes in the S_1 state of **1**−**3** were completed in the first ≈600−800 fs. After that, the induced optical density slowly relaxed to zero in accordance with the nanosecond lifetimes τ_{fl} of the corresponding S_1 states (see Table 1). It should be mentioned that negative values of ΔD indicate a dominant role of SA effect in the main absorption bands of **1**−**3**. In the fluorescence spectral range ($\lambda_{pr} \geq$ 440 nm, see Figure 5), transient absorption curves revealed specific fast relaxations on the ∼1−2 ps time scale, and a major contribution of ESA processes (positive ΔD) can be assumed. Observed fast relaxations were of a different sign: increase in ΔD was obtained for λ_{pr} = 495, 505, and 515 nm (Figure 5a, d, g), and decrease was obtained for λ_{pr} = 575, 626, and 615 nm (Figure 5c, f, i), which is indicative of the hypsochromic shift of the instantaneous ESA spectra of **1**−**3** in polar ACN. Corresponding time-resolved ESA spectra are presented in Figure 6 for several values of τ_D.

According to this data, the observed hypsochromic shifts were completed in the first 5 ps after electronic excitation $S_0 \rightarrow S_1$ and can be attributed to the solvate relaxation phenomena,[11,31] resulting in the larger stabilization of the S_1 state in **1**−**3** relative to the higher excited S_n state participating in ESA processes. The largest hypsochromic shift was observed in **3**, which is characterized by a D-π-A structure and the largest changes in the permanent dipole moment under $S_0 \rightarrow S_1$ electronic excitation. It should be mentioned that higher excited states S_n typically exhibit much less efficient dependence on solvent polarity due to a locally excited character of these states.[32]

3.3. Quantum Chemical Description of the Electronic Properties of 1−3. Optimized molecular geometries of **1**−**3** in polar ACN were calculated at the M05-QX/D95 theory level using a PCM model in SMD parametrization[26] and presented in Figure 7 for the ground electronic state S_0. Previously we had demonstrated that PCM is sufficiently accurate for description of solvatochromic effects in aprotic and weakly acidic

dx.doi.org/10.1021/jp503263f | J. Phys. Chem. A XXXX, XXX, XXX−XXX

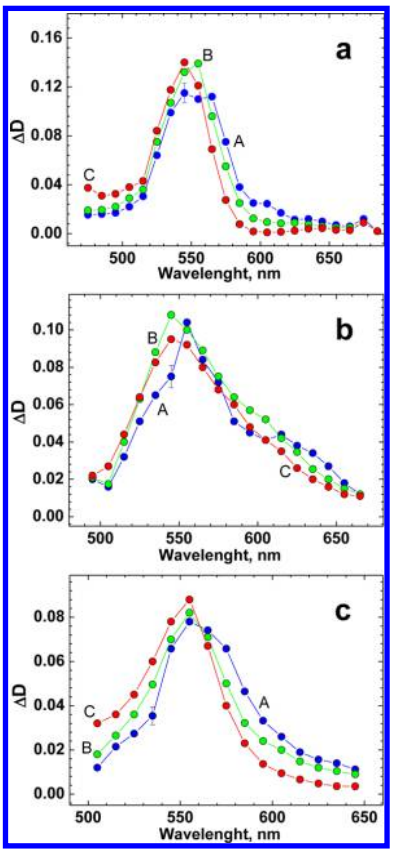

Figure 6. Time-resolved ESA spectra of **1** (a), **2** (b), and **3** (c) in ACN for τ_D = 0.6 ps (A), 1 ps (B), and 5 ps (C).

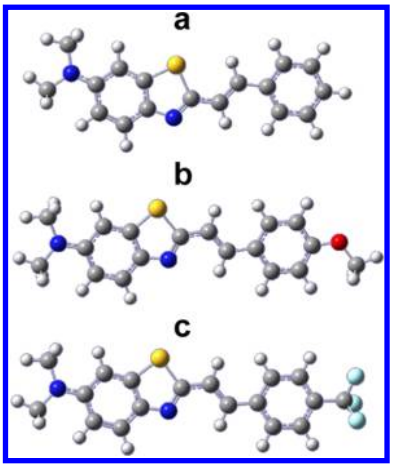

Figure 7. Optimized molecular geometry of **1** (a), **2** (b), and **3** (c) in ACN in the S_0 electronic state.

solvents,[33] while explicit solvent molecules may be necessary in case of more acidic ones.[19,20] As follows from the performed calculations molecular structures of **1**−**3** are planar except for the methyl and trifluoromethyl terminal groups, including sp^3-hybridized carbons. It should be mentioned that the calculated optimized geometry of **1**−**3** in the first excited state S_1 remains planar with noticeable changes in bond length alternation (BLA)[34] of the π-conjugated system (see Figure 8), which can be attributed to dramatic changes in the potential surface of the excited state and corresponding large Stokes shifts in nonpolar solvents.[35,36] Calculated electronic parameters of **1**−**3** in ACN, including transition dipoles and main orbital configurations, are presented in Table 2, where HOMOs and LUMOs represent

Table 2. Calculated Electronic Parameters of 1−3 in ACN and Main Orbital Configurations: Absorption Maxima λ_{cal}^{abs}, Oscillator Strengths f_{OS}, Changes in the Permanent Dipole Moments under Electronic Excitation $S_0 \rightarrow S_i$ $|\Delta\mu_{0i}|$, and Corresponding Transition Dipole Moments μ_{0i} (i = 1−3)

compd	transitions	λ_{cal}^{abs}, nm	fOS	$\lvert\Delta\mu_{0i}\rvert$, D	μ_{0i}, D	main configurations
1	$S_0 \rightarrow S_1$	409	1.17	14.04	8.03	0.95 |HOMO → LUMO⟩
	$S_0 \rightarrow S_2$	301	0.22	5.72	0.90	0.92|HOMO−1 → LUMO⟩
	$S_0 \rightarrow S_3$	287	0.09	1.30	0.17	−0.30|HOMO−2 → LUMO⟩
						0.35|HOMO → LUMO+1⟩
						0.39|HOMO → LUMO+2⟩
2	$S_0 \rightarrow S_1$	404	1.31	10.89	8.65	0.98|HOMO → LUMO ⟩
	$S_0 \rightarrow S_2$	312	0.36	0.25	1.16	0.95|HOMO−1 → LUMO⟩
	$S_0 \rightarrow S_3$	289	0.03	1.08	0.18	–
3	$S_0 \rightarrow S_1$	435	1.03	17.99	7.50	0.77|HOMO → LUMO⟩
	$S_0 \rightarrow S_2$	308	0.39	9.50	1.65	0.95|HOMO−1 → LUMO⟩
	$S_0 \rightarrow S_3$	287	0.20	3.08	0.39	−0.34|HOMO−2 → LUMO⟩
						0.58|HOMO → LUMO+3⟩

the highest occupied molecular orbitals and the lowest unoccupied molecular orbitals, respectively. The essential molecular orbitals involved in $S_0 \rightarrow S_i$ transitions (i = 1−3) are shown in Table 3. Deduced from the data in Tables 2, 3, the first electronic transitions $S_0 \rightarrow S_1$ of **1**−**3** can be attributed to the main long wavelength absorption bands of the compounds and nicely correspond to the experimental absorption maxima

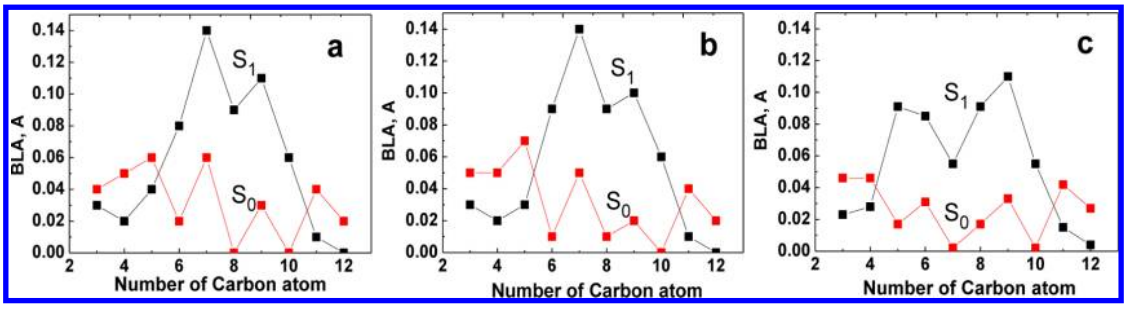

Figure 8. Calculated BLA values for the optimized geometries of **1** (a), **2** (b), and **3** (c) in the ground S_0 and first excited S_1 electronic state.

dx.doi.org/10.1021/jp503263f | J. Phys. Chem. A XXXX, XXX, XXX−XXX

Table 3. Main Molecular Orbitals of 1−3

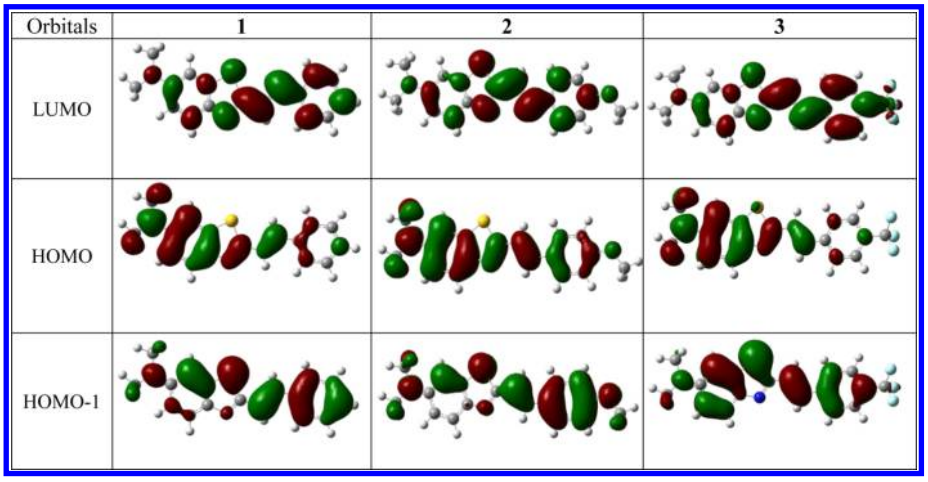

λ_{ab}^{max} shown in Table 1. These transitions are of $\pi-\pi^*$ nature with oscillator strengths in the range $f_{OS} \approx 1.0-1.3$ and corresponding transition dipole moments $\boldsymbol{\mu}_{01} \approx 7.5-8.7$ D. It is worth mentioning that the calculated values of $\boldsymbol{\mu}_{01}$ are comparable to the experimental ones $\boldsymbol{\mu}_{01}^{exp} \approx 8.1$ D (**1**), 8.4 D (**2**), and 7.5 D (**3**), obtained from integration of the experimental absorption spectra: $\boldsymbol{\mu}_{01} \approx 0.096 \cdot \int \varepsilon(\nu) \cdot d\nu / \nu^{max}$,[34] where μ_{01} is in D, $\varepsilon(\nu)$ is in M^{-1} cm^{-1}, ν and $\nu^{max} = 1/\lambda_{ab}^{max}$ are in cm^{-1}. The only one bright electronic transition $S_0 \rightarrow S_1$ of **1**−**3** ($\lambda_{cal}^{abs} \approx 400-430$ nm) is consistent with the constant experimental values of anisotropies observed in the spectral range 350−470 nm (Figure 3, curves 4). As it follows from the calculations, the second $\boldsymbol{\mu}_{02}$ and third $\boldsymbol{\mu}_{03}$ transition dipole moments of **1**−**3** are not collinear with $\boldsymbol{\mu}_{01}$ that explains the decrease in anisotropy at $\lambda < 350$ nm. The minor absorption maximum in Figure 3b and shoulders in Figure 3a, c in the range $\lambda \approx 300-325$ nm apparently correspond to substantially darker electronic transition $S_0 \rightarrow S_2$ with oscillator strengths in the range $f_{OS} \approx 0.2-0.4$. Optimized molecular geometry of the first excited state S_1 (calculated with PCM model in SMD parametrization using TD-DFT approach) allows one to estimate fluorescence emission maxima, λ_{cal}^{fl}, in polar ACN. Obtained values of λ_{cal}^{fl} = 545 nm (**1**), 544 nm (**2**), and 577 nm (**3**) are in agreement with corresponding experimental ones λ_{fl}^{max} (see Table 1).

Our calculations rationalize the observed differences in solvatochromic shifts between absorption and emission in the following way. The excitation of the chromofores **1**−**3** into S_1 state is accompanied by the strong charge transfer, increasing the permanent dipole moment of the molecule from 2 D to over 9 D (see Table 2). Therefore, orientational solvent reaction field generated by the excited solute during the emission process, is four- to sixfold stronger than the reaction field generate by the ground state during the absorption process. This explains why the extra stabilization of the more polar excited state, manifested by solvatochromic shift, is much more pronounced during emission than it was during absorption.

4. CONCLUSIONS

The synthesis and comprehensive steady-state and time-resolved pico- and femtosecond investigations of the photophysical properties of new styryl base-types derivatives were performed. The steady-state spectroscopic parameters indicated on a strong rearrangement of the optimized molecular geometry of **1**−**3** in the first excited electronic state S_1 resulting in the large Stokes shift in nonpolar solvent. Excitation anisotropy spectra revealed only one electronic transition, which can be related to the main long wavelength absorption bands of **1**−**3** and nearly parallel orientation of the absorption $\boldsymbol{\mu}_{01}$ and emission $\boldsymbol{\mu}_{10}$ transition dipole moments. All linear spectroscopic data were in good agreement with TD-DFT calculations performed with the use of a polarizable continuum model, indicative of the high predictive ability of this approach for future optical materials design. Fast relaxation processes in the S_1 state of **1**−**3** were observed in polar ACN on a time scale of 1−2 ps and can be attributed to solvate reorientation dynamics resulting in the observed hypsochromic shift in the time-resolved ESA spectra. The spectroscopic investigations of steady-state and time-resolved photophysical properties of these new styryl dye bases have potential for the further development of a number of areas including biosensing, bioimaging, and organic photovoltaics.

AUTHOR INFORMATION

Corresponding Authors

* E-mail: amasunov@gmail.com. Phone: +011 (407) 882-0195.
*E-mail: mbondar@mail.ucf.edu. Phone: +38 (044) 525-9968.

Notes

The authors declare no competing financial interest.

ACKNOWLEDGMENTS

The authors thank the employees of the NASU Center for collective use of "Laser femtosecond complex". This work is supported in part by the National Academy of Sciences of Ukraine (grants 1.4.1.B/153 and VC/157). A.E.M. acknowledges the use of computational resources at The Stokes Advanced Research Computing Center, University of Central Florida (UCF), and the National Energy Research Scientific Computing Center, which is supported by the Office of Science of the U.S. Department of Energy under Contract No. DE-AC02-05CH11231. K.D.B. acknowledges the National Science Foundation (CHE-08).

REFERENCES

(1) Rettig, W.; Rurack, K.; Sczepan, M. From Cyanine to Styryl Bases—Photophysical Properties, Photochemical Mechanisms, and Cation Densing Abilities of Charged and Neutral Polymethinic Dyes.

In *New Trends in Fluorescence Spectroscopy: Applications to Chemical and Life Sciences*; Valeor, B., Bredas, J.-L., Eds.; Springer: Berlin, 2001; pp 125−155.
(2) Kakuta, A.; Mori, Y.; Morishita, H. The Ionization Potential of Carrier Transport Materials in Relation to the Photosensitivity of Double Layered Photoreceptors. *IEEE Trans. Ind. Appl.* **1981**, *IA−17*, 382−386.
(3) Li, Q.; Min, J.; Ahn, Y.-H.; Namm, J.; Kim, E. M.; Lui, R.; Kim, H. Y.; Ji, Y.; Wu, H.; Wisniewski, T.; et al. Styryl-Based Compounds as Potential in Vivo Imaging Agents for B-Amyloid Plaques. *ChemBioChem* **2007**, *8*, 1679−1687.
(4) Yuan, M. J.; Li, Y. J.; Liu, H. B.; Li, Y. L. Chemical Sensors Based on π-Conjugated Organic Molecules and Gold Nanoparticles. *Sci. China, Ser. B: Chem.* **2009**, *52*, 715−730.
(5) Egbe, D. A. M.; Tekin, E.; Birckner, E.; Pivrikas, A.; Sariciftci, N. S.; Schubert, U. S. Effect of Styryl Side Groups on the Photophysical Properties and Hole Mobility of PPE−PPV Systems. *Macromolecules* **2007**, *40*, 7786−7794.
(6) Bricks, J. L.; Slominskii, J. L.; Kudinova, M. A.; Tolmachev, A. I.; Rurack, K.; Resch-Genger, U.; Rettig, W. Syntheses and Photophysical Properties of a Series of Cation-Sensitive Polymethine and Styryl Dyes. *J. Photochem. Photobiol., A* **2000**, *132*, 193−208.
(7) Vembris, A.; Muzikante, I.; Karpicz, R.; Sliauzys, G.; Miasojedovas, A.; Jursenas, S.; Gulbinas, V. Fluorescence and Amplified Spontaneous Emission of Glass Forming Compounds Containing Styryl-4*H*-pyran-4-ylidene Fragment. *J. Lumin.* **2012**, *132*, 2421−2426.
(8) Fayed, T. A.; Etaiw, S. H.; Khatab, H. M. Excited State Properties and Acid−Base Equilibria of *trans*-2-Styrylbenzoxazoles. *J. Photochem. Photobiol., A* **2005**, *170*, 97−103.
(9) Frisch, M. J.; Trucks, G. W.; Schlegel, H. B.; Scuseria, G. E.; Robb, M. A.; Cheeseman, J. R.; Scalmani, G.; Barone, V.; Mennucci, B.; Petersson, G. A.; et al. *Gaussian 09*, revision D.01; Gaussian, Inc.: Wallingford, CT, 2009.
(10) Rurack, K.; Koval'chuck, A.; Bricks, J. L.; Slominskii, J. L. A Simple Bifunctional Fluoroionophore Signaling Different Metal Ions Either Independently or Cooperatively. *J. Am. Chem. Soc.* **2001**, *123*, 6205−6206.
(11) Lakowicz, J. R. *Principles of Fluorescence Spectroscopy*; Kluwer: New York, 1999.
(12) Belfield, K. D.; Bondar, M. V.; Hales, J. M.; Morales, A. R.; Przhonska, O. V.; Schafer, K. J. One- and Two-Photon Fluorescence Anisotropy of Selected Fluorene Derivatives. *J. Fluoresc.* **2005**, *15*, 3−11.
(13) Fu, J.; Przhonska, O. V.; Padilha, L. A.; Hagan, D. J.; Van Stryland, E. W.; Belfield, K. D.; Bondar, M. V.; Slominsky, Y. L.; Kachkovski, A. D. Two-Photon Anisotropy: Analytical Description and Molecular Modeling for Symmetrical and Asymmetrical Organic Dyes. *Chem. Phys.* **2006**, *321*, 257−268.
(14) Lepkowicz, R. S.; Przhonska, O. V.; Hales, J. M.; Hagan, D. J.; Van Stryland, E. W.; Bondar, M. V.; Slominsky, Y. L.; Kachkovski, A. D. Excited-State Absorption Dynamics in Polymethine Dyes Detected by Polarization-Resolved Pump−Probe Measurements. *Chem. Phys.* **2003**, *286*, 277−291.
(15) Miyasaka, H.; Murakami, M.; Okada, T.; Nagata, Y.; Itaya, A.; Kobatake, S.; Irie, M. Picosecond and Femtosecond Laser Photolysis Studies of a Photochromic Diarylethene Derivative: Multiphoton Gated Reaction. *Chem. Phys. Lett.* **2003**, *371*, 40−48.
(16) Dunning, T. H.; Hay, P. J. In *Modern Theoretical Chemistry*; Schaefer, H. F., III, Ed.; 1977; Vol. 3, pp 1−21.
(17) Mikhailov, I. A.; Bondar, M. V.; Belfield, K. D.; Masunov, A. E. Electronic Properties of a New Two-Photon Absorbing Fluorene Derivative: The Role of Hartree−Fock Exchange in the Density Functional Theory Design of Improved Nonlinear Chromophores. *J. Phys. Chem. C* **2009**, *113*, 20719−20724.
(18) Zhao, Y.; Schultz, N. E.; Truhlar, D. G. Design of Density Functionals by Combining the Method of Constraint Satisfaction with Parametrization for Thermochemistry, Thermochemical Kinetics, and Noncovalent Interactions. *J. Chem. Theory Comput.* **2006**, *2*, 364−382.
(19) De Boni, L.; Toro, C.; Masunov, A. E.; Hernandez, F. E. Untangling the Excited States of DR1 in Solution: An Experimental and Theoretical Study. *J. Phys. Chem. A* **2008**, *112*, 3886−3890.
(20) Toro, C.; Thibert, A.; De Boni, L.; Masunov, A. E.; Hernandez, F. E. Fluorescence Emission of Disperse Red 1 in Solution at Room Temperature. *J. Phys. Chem. B* **2008**, *112*, 929−937.
(21) Mikhailov, I. A.; Belfield, K. D.; Masunov, A. E. DFT-Based Methods in the Design of Two-Photon Operated Molecular Switches. *J. Phys. Chem. A* **2009**, *113*, 7080−7089.
(22) Liu, J. H.; Mikhaylov, I. A.; Zou, J. H.; Osaka, I.; Masunov, A. E.; McCullough, R. D.; Zhai, L. Insight into How Molecular Structures of Thiophene-Based Conjugated Polymers Affect Crystallization Behaviors. *Polymer* **2011**, *52*, 2302−2309.
(23) Nayyar, I. H.; Masunov, A. E.; Tretiak, S. Comparison of TD-DFT Methods for the Calculation of Two-Photon Absorption Spectra of Oligophenylvinylenes. *J. Phys. Chem. C* **2013**, *117*, 18170−18189.
(24) Masunov, A. E.; Mikhailov, I. A. Theory and Computations of Two-Photon Absorbing Photochromic Chromophores. *Eur. J. Chem.* **2010**, *1*, 142−161.
(25) Casida, M. E.; Huix-Rotllant, M. Progress in Time-Dependent Density-Functional Theory. *Annu. Rev. Phys. Chem.* **2012**, *63*, 287−323.
(26) Marenich, A. V.; Cramer, C. J.; Truhlar, D. G. Universal Solvation Model Based on Solute Electron Density and on a Continuum Model of the Solvent Defined by the Bulk Dielectric Constant and Atomic Surface Tensions. *J. Phys. Chem. B* **2009**, *113*, 6378−6396.
(27) Strickler, S. J.; Berg, R. A. Relationship between Absorption Intensity and Fluorescence Lifetime of Molecules. *J. Chem. Phys.* **1962**, *3*, 814−822.
(28) Kosumi, D.; Maruta, S.; Fujii, R.; Kanemoto, K.; Sugisaki, M.; Hashimoto, H. Ultrafast Excited State Dynamics of Monomeric Bacteriochlorophyll A. *Phys. Status Solidi C* **2011**, *8*, 92−95.
(29) Fita, P.; Fedoseeva, M.; Vauthey, E. Ultrafast Excited-State Dynamics of Eosin B: A Potential Probe of the Hydrogen-Bonding Properties of the Environment. *J. Phys. Chem. A* **2011**, *115*, 2465−2470.
(30) Golibrzuch, K.; Ehlers, F.; Scholz, M.; Oswald, R.; Lenzer, T.; Oum, K.; Kim, H.; Koo, S. Ultrafast Excited State Dynamics and Spectroscopy of 13,13′-Diphenyl-*B*-carotene. *Phys. Chem. Chem. Phys.* **2011**, *13*, 6340−6351.
(31) Horng, M. L.; Gardecki, J. A.; Papazyan, A.; Maroncelli, M. Subpicosecond Measurements of Polar Solvation Dynamics: Coumarin 153 Revisited. *J. Phys. Chem.* **1995**, *99*, 17311−17337.
(32) Viniychuk, O. O.; Levchenko, S. M.; Przhonska, O. V.; Kachkovsky, O. D.; Bricks, Y. L.; Kudinova, M. O.; Kovtun, Y. P.; Poronik, Y. M.; Shandura, M. P.; Tolmachev, O. I. Electronic Transitions in Polymethine Dyes Involving Local and Delocalized Levels. *J. Mol. Struct.* **2014**, *1060*, 30−37.
(33) Masunov, A.; Tretiak, S.; Hong, J. W.; Liu, B.; Bazan, G. C. Theoretical Study of the Effects of Solvent Environment on Photophysical Properties and Electronic Structure of Paracyclophane Chromophores. *J. Chem. Phys.* **2005**, *122*, 224505/1−10.
(34) Hales, J. M.; Matichak, J.; Barlow, S.; Ohira, S.; Yesudas, K.; Brédas, J.-L.; Perry, J. W.; Marder, S. R. Design of Polymethine Dyes with Large Third-Order Optical Nonlinearities and Loss Figures of Merit. *Science* **2010**, *327*, 1485−1488.
(35) Tanaka, K.; Komiya, T. Novel Fluorescent 2-(2-Aminofluorophenyl)Benzoxazoles: Syntheses and Photophysical Properties. *J. Heterocycl. Chem.* **2002**, *39*, 1299−1304.
(36) Casteel, D. A.; Leonard, N. J. Synthesis of Pyrrolo[3,4-D]Imidazoles. A New Fluorescent Heterocyclic System. *J. Org. Chem.* **1985**, *50*, 2450−2456.